Proceedings of ASME Turbo Expo 2008: Power for Land, Sea and Air
GT2008
June 9-13, 2008, Berlin, Germany

GT2008-50779

NUMERICAL INVESTIGATION OF RELATION BETWEEN UNSTEADY BEHAVIOR OF TIP LEAKAGE VORTEX AND ROTATING DISTURBANCE IN A TRANSONIC AXIAL COMPRESSOR ROTOR

K. Yamada, K. Funazaki, and H. Sasaki
Department of Mechanical Engineering
Iwate University
Morioka, 020-8551, Japan

ABSTRACT

The purpose of this study is to have a better understanding of the unsteady behavior of tip clearance flow at near-stall condition from a multi-passage simulation and to clarify the relation between such unsteadiness and rotating disturbance. This study is motivated by the following concern. A single passage simulation has revealed the occurrence of the tip leakage vortex breakdown at near-stall condition in a transonic axial compressor rotor, leading to the unsteadiness of the tip clearance flow field in the rotor passage. These unsteady flow phenomena were similar to those in the rotating instability, which is classified in one of the rotating disturbances. In other words , it is possible that the tip leakage vortex breakdown produces a rotating disturbance such as the rotating instability. Three-dimensional unsteady RANS calculation was conducted to simulate the rotating disturbance in a transonic axial compressor rotor (NASA Rotor 37). The four-passage simulation was performed so as to capture a short length scale disturbance like the rotating instability and the spike-type stall inception. The simulation demonstrated that the unsteadiness of tip leakage vortex, which was derived from the vortex breakdown at near-stall condition, invoked the rotating disturbance in the rotor, which is similar to the rotating instability.

INTRODUCTION

The rotating stall and surge are known as an unsteady flow phenomenon observed in compressors. They are responsible for noise generation and excitation of blade vibration in a compressor, and therefore the compressor may suffer from a fatigue failure of the blade and will eventually become unable to be operated. Consequently, the unsteady flow phenomena at rotating stall inception in axial compressors have been investigated by many researchers. It has been found that there are two types of the rotating disturbances at stall inception in axial compressors: 'spike' mode and 'modal' mode [1–3]. It was suggested that the spike-type disturbance was related to local separation of the boundary layer on the blade suction surface near the rotor tip [4], and also it might be explained by a behavior of the tip leakage vortex moving upstream of the rotor with the incidence increasing [5]. Hah et al. have conducted unsteady three-dimensional numerical simulation for a low speed axial compressor and noted the relation between the tip leakage vortex and the rotating disturbance [6]. Criteria for the spike stall have been proposed from the results of single-passage simulations on various compressor rotors; they are 'backflow' at the trailing edge and 'spillage' of leading edge flow in tip region [7].

It has been found, however, that there are other routes of stall evolution, that is so-called 'high frequency stall inception' which has been observed by Day et al. [8]. The high frequency waves are considered to result from multiple short length-scale part-span stall cells, structure of which has been elucidated by Inoue et al [9, 10]. In addition, other unsteady flow phenomena have been observed at near-stall condition in experimental and numerical studies. Mailach et al. have observed the rotating instability in a low-speed axial compressor with relatively large tip clearances of rotor [11]. The explanation was that the fluctuation of tip leakage vortex could be responsible for the origina-

tion of that unsteady flow phenomenon. Numerical studies have shown that the vortex breakdown gave rise to an unsteadiness in the tip leakage vortex [12, 13]. The breakdown of tip leakage vortex occurred at near-stall condition, and it not only brought about the unsteadiness, but produced a large blockage and reversed flow in rotor tip region. It was able to account nicely for the anomalous flow phenomena observed in the experiment [14]. The occurrence of the tip leakage vortex breakdown was also confirmed at near-stall condition in a transonic axial compressor rotor [15,16]. Although it is considered that the above-mentioned unsteady flow phenomena are related to the tip leakage vortex, the details of the flow field in the presence of the unsteady flow phenomena remain unsolved. Especially, high-speed compressors lack sufficient unsteady data from the experiment in terms of the flow field inside the rotor. That is why these unsteady flow phenomena does not definitely seem to be distinguishable from each other. However, there seem to be a common feature between the unsteady flow phenomena due to the vortex breakdown and the rotating instability, that is the unsteady behavior of tip leakage vortex.

The purpose of the present work is to investigate details of the unsteady behavior of tip clearance flow at near-stall condition from a multi-passage simulation and to clarify the relation between such unsteadiness and the rotating disturbance, especially the rotating instability. The unsteady flow field near the rotor tip in the transonic axial compressor rotor have been investigated by a multi-passage unsteady RANS simulation and by a method of identifying vortex structures based on the critical-point theory. In this paper, the rotating instability is used to distinguish from the other short length-scale rotating disturbance. The rotating instability is defined here as the rotating disturbance that does not grow to a fully developed rotating stall. The rotating disturbance is used as the generic term for all types of disturbances to be observed in compressors.

TRANSONIC COMPRESSOR ROTOR

A transonic axial compressor rotor, NASA Rotor 37, was used for the present work. The rotor was originally designed as an inlet rotor for a core compressor and tested at NASA Lewis Research Center in the late 1970's [17]. The specification of the rotor is summarized in Table 1. The rotor design pressure ratio is 2.106 at a mass flow of 20.19kg/s. The inlet relative Mach number is 1.13 at the hub and 1.48 at the tip at the design speed of 454m/s (17,188.7rpm). The rotor has 36 blades with a hub-tip ratio of 0.7, an aspect ratio of 1.19, and a tip solidity of 1.288. The tip clearance is 0.356mm. The rotor was re-tested in a single-stage compressor facility, which was described in [18]. This rotor was used for the ASME code assessment 'blind test case' at the ASME/IGTI 39th International Gas Turbine Conference [19]. The simulations were compared to these experimental data [20–22]. Figure 1 shows the location measured using pneumatic probes and laser anemometer system, where radial distributions of static and total pressure, and total temperature, and velocity distributions at some blade-to-blade planes were obtained.

Table 1. Design specification of test compressor

Blade number	36
Radius of tip at leading edge	252mm
Aspect ratio	1.19
Solidity at tip	1.288
Tip clearance	0.356mm (0.45% span)
Hub-tip ratio	0.7
at design	
Tip speed	454m/s (17,188.7rpm)
Total pressure ratio	2.106
Massflow	20.19kg/s
Choke massflow	20.93kg/s

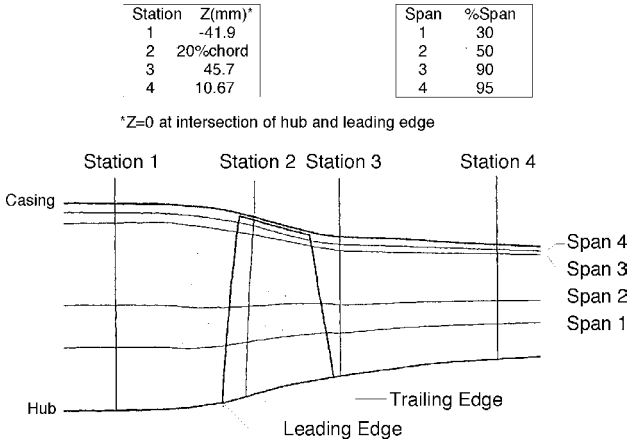

Figure 1. Measurement locations in experiment

NUMERICAL ANALYSIS METHOD

Numerical scheme

The simulations were performed by solving the compressible Navier-Stokes equations using an unfactored implicit upwind relaxation scheme with inner iterations [23, 24]. The numerical method used in the present flow solver is outlined in the following. The three-dimensional Reynolds-averaged Navier-Stokes equations were discretized in space using a cell-centered finite volume formulation and in time using the Euler implicit method. The inviscid fluxes were evaluated by the simple high-resolution upwind scheme (SHUS) [25], which was extended to third-order accurate by the MUSCL interpolation with the Van Albada limiter [26]. The viscous fluxes were determined in a central differencing manner with Gauss's theorem. As for turbulence model, the k-ω turbulence model [27] was employed to estimate the eddy viscosity. A point Gauss-Seidel relaxation

method using no approximate factorization was used in time integration [23]. To obtain a time-accurate solution in the unsteady flow simulations, inner iterations, so-called Newton iterations, were introduced at each time step according to Chakravarthy [28]. The scheme achieved up to second-order accurate in time by applying the three-point-backward difference approximation to the temporal derivative [24]. In the present work, seven inner iterations were performed at each time step, and a nondimensional time step size normalized by the rotor tip radius and the inlet sound speed was set to 0.00005. More than 2,500 time steps were included in the blade passing period that was taken for a rotor blade to pass through one pitch. For the treatment of boundary condition, fictitious cells were introduced just outside all the boundaries of computation domain. The experimental data measured at Station 1 (shown in Fig.1) was used for the inflow boundary. At the outflow boundary, all the physical quantities were extrapolated from the interior to the fictitious cells and the magnitude of the velocity in the cells was scaled so as to maintain the imposed total mass flow rate.

Computational grid

The purpose of this work is to investigate the relation between the unsteady behavior of tip leakage vortex and the rotating instability. An annulus simulation should be executed in principle for such study [29, 30]. However, it turned out to be impossible for the lack of computational resource to carry out the annulus simulation while keeping the grid resolution enough to sharply capture the tip leakage vortex. The circumferential extent of the unsteady simulation was restricted to four rotor passages to save computational resource and time. It was believed that this computational domain had size enough to capture a short length-scale disturbance like the rotating instability. The circumferential wavelength of the rotating instability is considered to be about 0.5-3.0 times the rotor blade pitch [11]. It should be noted that the four-passage simulation constrained the disturbances to be appeared in the rotor as compared to the annulus simulation (36-passage simulation in the present case). The disturbances are required to match the four-passage periodicity. The wave length of the disturbance, which satisfies the 36-passage periodicity but not the four-passage periodicity, is possibly changed to fit the four-passage periodicity. However, it is expected that even the four-passage simulation will not make much difference on the mechanism or the flow physics of the disturbance. Because, the rotating instability is considered to be a result from the fluctuation of tip leakage vortex in the rotor passage. The main concern of the work is to show a possibility for an occurrence of the rotating instability induced by the unsteady flow phenomena due to the tip leakage vortex breakdown.

The computational grid is shown in Fig. 2. The multi-block grid system was employed to the present simulations. Structured H-type grid were generated upstream and downstream of the rotor. The grids consisted of 19 points in the streamwise direction, 110 points in the spanwise direction, and 46 points in the pitchwise direction. An O-type grid was used around the blade, and consisted of 179 points around the blade, 51 points in the direction perpendicular to the blade, and 110 points in the spanwise direction. In terms of the spanwise distribution of the grids, grid resolution was set to high near the rotor tip in order to capture the tip leakage flow field accurately. Furthermore, a H-type grid was used in the tip clearance region with 84 points in the chordwise direction, 26 points in the radial direction and 31 points in the pitchwise direction. Small blocks of H-type grid were embedded in the leading edge and trailing edge of the tip clearance to prevent a singular point from appearing. The total grid of one rotor passage had 1,340,702 points, which resulted in 5,362,808 points in four rotor passages. The ratio of the minimum grid spacing on solid walls to the blade tip chord length was less than 1.0×10^{-5} to evaluate the viscous fluxes at the walls by applying the no-slip and adiabatic conditions with no wall function method. This minimum grid spacing gave $y^+ < 1$ at the walls.

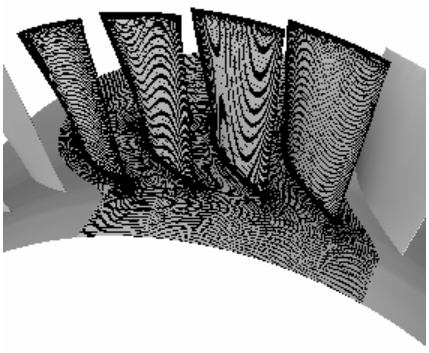

(a) Overview

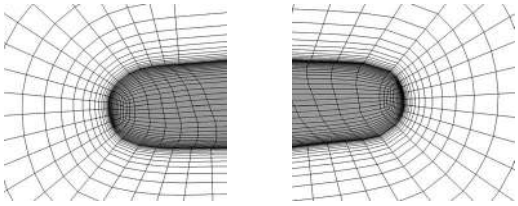

(b) Up-close view of the leading edge and trailing edge

Figure 2. Computational grid

Visualization Method

Visualization of vortical structures can be of help for understanding complicated flow field like in compressor rotors. It is hard to have a clear grasp of such complicated flow field by conventional flow visualization techniques such as particle traces, contour plots, secondary vector plots and so on. In addition, the streamline may lead to misinterpretation of the flow field since it corresponds with neither the streak line nor path line in unsteady

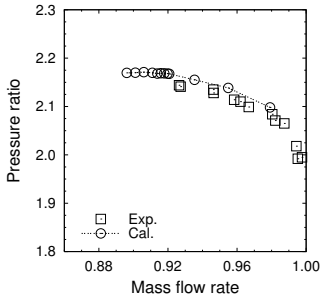

Figure 3. Total pressure ratio characteristics of rotor

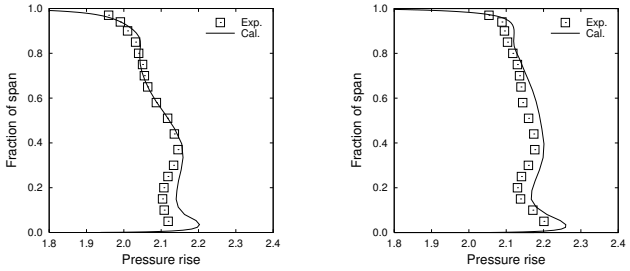

(a) Near-peak efficiency condition (b) Near-stall condition

Figure 4. Spanwise distributions of total pressure ratio

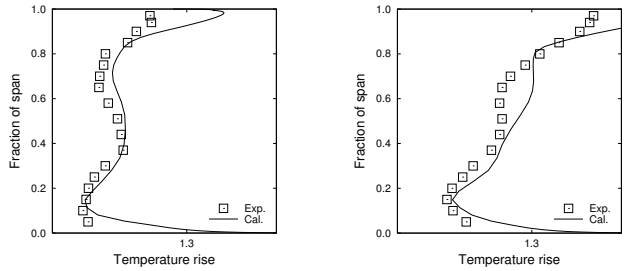

(a) Near-peak efficiency condition (b) Near-stall condition

Figure 5. Spanwise distributions of total temperature ratio

flow field. Therefore, it is critical to identify the vortex structure for the purpose of revealing details of the tip clearance flow field in the transonic axial compressor rotor.

A trajectory of the vortex core is identified by a semi-analytic method developed by Sawada [31]. In his method, assuming that a local velocity field can be linearly parameterized in a tetrahedral computational cell, streamline equations become integrable analytically for the cell, and as a result the obtained streamline expression provides a possible vortex centerline in the cell. In the present study, each hexahedral computational cell is divided into five tetrahedrons to apply Sawada's method. The computational cell crossed by the vortex center line is then regarded as a fraction of the vortex core. The value of unity is given at each vertex of the cells crossed by the vortex center, and zero at the vertices of the other cells. An iso-surface of the specified value is drawn to represent the whole vortex core structure.

Simulation Procedure

The total pressure ratio characteristics are shown in Fig. 3. Simulations for the rotating disturbance should be started from proper initial condition because of the hysteresis of rotating stall. In the present study, a steady-state or quasi-steady state solution at a little higher mass flow rate was used as the initial condition for the simulations. At first, a simulation was performed at a near-peak efficiency condition (98% mass flow rate). The mass flow rate was reduced by 2 percent each simulation from the near-peak efficiency condition toward stall in order to consider the context where the compressor rotor is throttled. The mass flow rate was fixed in each simulation. Since the flow field is considered to be almost in a steady-state before the disturbance occurs, steady-state simulations for a single passage of the rotor have been carried out as long as the simulation could converge to a steady-state solution. At less than 92% mass flow rate, the steady-state solution could not be obtained from the steady-state simulation. Accordingly, the unsteady simulations of four rotor passages were performed below 92% mass flow rate and the mass flow rate decreased more gradually. It is believed that the stall point of the rotor from the experiment is nearly 91.9% mass flow rate. However, in the present simulation the stall and any rotating disturbances didn't happen even at 90% mass flow rate although an unsteadiness appeared in the rotor passage. Therefore, the mass flow rate was reduced down to 88% mass flow rate. At this mass flow rate, the simulation showed an unsteady flow field different from that at 90% mass flow rate and a disturbance propagating across the passages. It should be noted that in the simulation at 88% mass flow rate an initial disturbance has been introduced at the early time (t = 8). The result in one of the passages was substituted for that at a different time. This special treatment can promote a rotating disturbance compared to the case without using the treatment. It was confirmed that the same disturbance appeared without such special treatment. All the results discussed below are from the unsteady simulation at 88% mass flow rate, except the results for validation.

RESULTS AND DISCUSSION

Validity of Numerical Simulation

In order to validate the simulation results obtained in the present work, comparisons are made between the numerical and experimental results with respect to two operating points of near-peak efficiency condition (98% mass flow rate) and near-stall condition (92.5% mass flow rate), at which the measurements has been performed. Figures 4 and 5 are a comparison of the numerical and experimental results in terms of the spanwise distributions of the total pressure ratio and total temperature ratio at station 4. The simulation results have a good agreement with

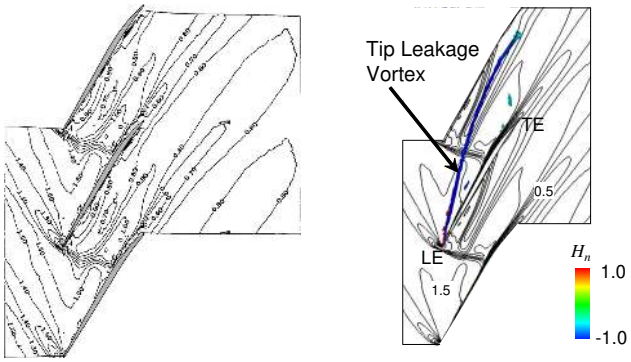

(a) Experiment (b) Calculation

Figure 6. Comparison of relative Mach number contour at 95% span at near-peak efficiency condition (vortex cores colored with normalized helicity are shown in calculation)

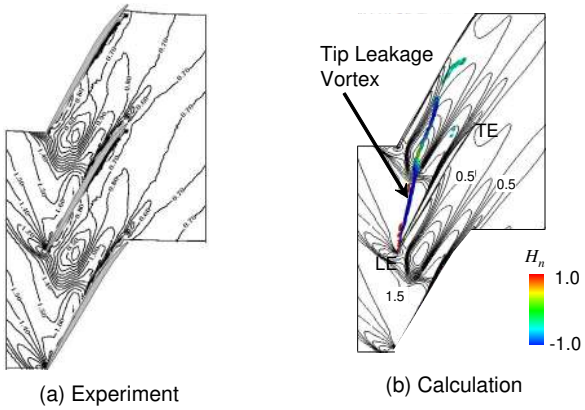

(a) Experiment (b) Calculation

Figure 7. Comparison of relative Mach number contour at 95% span at near-stall condition (vortex cores colored with normalized helicity are shown in calculation)

the experiments. Especially, as shown in Fig. 4, the simulations have succeeded in predicting a deficit near the hub in the total pressure profiles although there is a quantitative difference in the deficit. It is considered that this discrepancy near the hub is attributed to the effect of the hub leakage flow that Shabbir et al. proposed [32]. The total temperature computed is somewhat overestimated at the near-stall condition. The simulations might have failed to accurately assess the loss from the shock-induced separation on the suction surface of the rotor blade, because the k-ω turbulence model was incapable of predicting such boundary layer separation exactly. The comparisons imply that the simulation has been able to predict the flow field with satisfactory accuracy.

Figures 6 and 7 show a comparison of the relative Mach number contour at 95% span. In the figure, vortical flow structures in the rotor are also shown for the calculation results. Vortex cores are identified according to the method above-mentioned

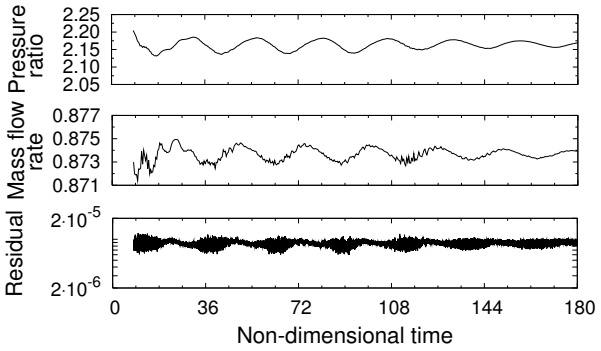

Figure 8. Time histories of total pressure rise, mass flow rate, and residual for the simulation at 88% mass flow rate

and are colored with the normalized helicity H_n defined as follows:

$$H_n = \frac{\vec{\xi} \cdot \vec{w}}{|\vec{\xi}||\vec{w}|} \tag{1}$$

where $\vec{\xi}$ and $\vec{w}$ denote vectors of the absolute vorticity and the relative flow velocity, respectively. The magnitude of the normalized helicity H_n takes the value of unity anywhere the streamwise vortex is present and it can assess the nature of vortex quantitatively, even when the vorticity decays. As seen from the experiment, a shock wave forms near the leading edge and interacts with the suction surface of the neighboring blade. A low-energy fluid, which has a blockage effect, appears just downstream of the shock wave. At the near-stall condition, the region of the low-energy fluid dramatically expands and the shock wave is bent in the rotor passage in comparison with the near-peak efficiency condition. The simulations are able to predict such flow phenomena. The simulations describe the interaction of the tip leakage vortex with the shock wave. The normalized helicity on the tip leakage vortex changes partly downstream of the shock wave at the near-stall condition. It has been explained that this implied the occurrence of the vortex breakdown in the tip leakage vortex [15, 16]. The vortex breakdown leads to a sudden expansion of the tip leakage vortex and even a reversed flow, which result in the large expansion of the low-energy fluid region at the near-stall condition.

Unsteady Behavior of Tip Leakage Vortex

The vortex breakdown has a large-scale unsteady nature. It should be realized that the breakdown of the tip leakage vortex, which has occurred at the near-stall condition, could induce unsteadinesses in the tip clearance flow field of the rotor. The unsteady flow behavior due to the vortex breakdown is described in this section. In the simulations, the vortex breakdown was observed below 92% mass flow rate. However, none of the rotating

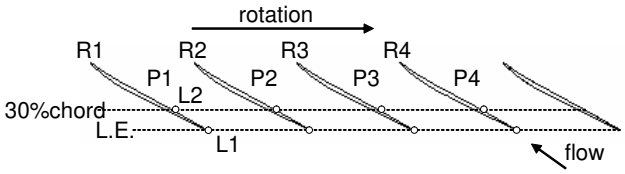

Figure 9. Illustration diagram of pressure sampling points and references to rotor and passage

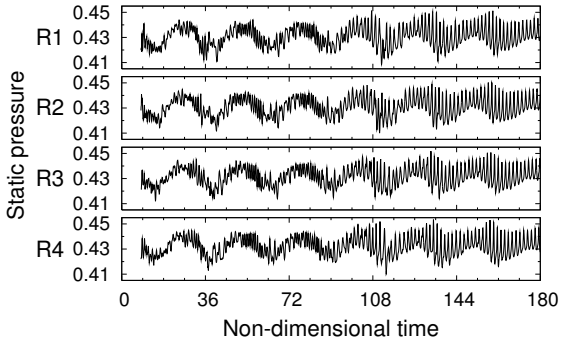

(a) Leading edge (L1)

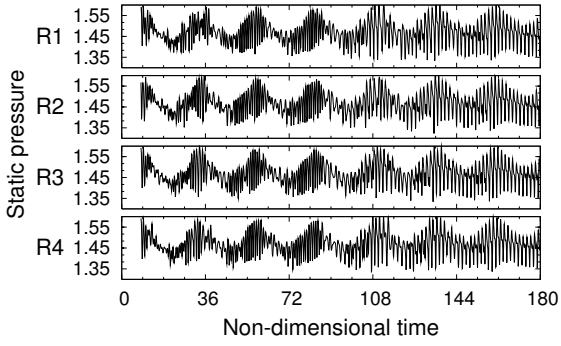

(b) 30% chord downstream from leading edge (L2)

Figure 10. Time history of static pressure on the blade pressure surface

disturbances appeared until 88% mass flow rate. Therefore, the discussion below about the unsteady flow is developed at 88% mass flow rate. Figure 8 shows time histories of total pressure ratio, mass flow rate, and residual in the simulation at 88% mass flow rate. In this paper, all the pressure were normalized by the inlet stagnation pressure, and all the time were normalized by the blade passing period. As shown in the figure, the fluctuations of total pressure ratio and mass flow rate were spawned at first in the simulation; however, they gradually decayed and the simulation converged to the quasi-steady state.

Figure 9 shows the data acquisition points of static pressure fluctuations on the pressure surface of the rotor blade. These points, L1 and L2, are located on the leading edge and 30% chord downstream from the leading edge near the blade tip, respectively. As shown in the figure, each of four rotors and passages

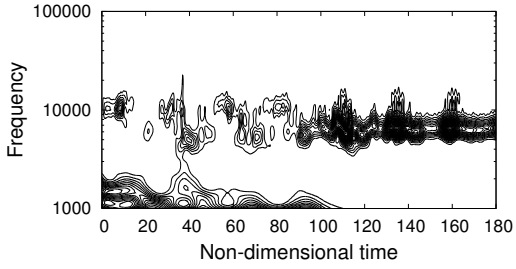

(a) L1

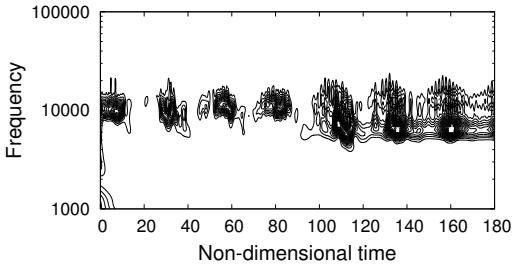

(b) L2

Figure 11. Wavelet transform of pressure fluctuation on the pressure surface (R4)

in the simulation is hereinafter referred to as R1 $\sim$ R4 and P1 $\sim$ P4. Figure 10 shows the pressure fluctuations at L1 and L2 of each blade. It should be noted that the data of the pressure fluctuations were obtained in the relative frame of reference fixed on the rotor, namely the data acquisition points moved with the rotor rotation. In the figures, high frequency fluctuations are attributed to an unsteady behavior of the tip leakage vortex. The tip leakage vortex, which has come to the vortex breakdown downstream of the shock wave, fluctuates with time near the adjacent blade tip as described later. The frequency of this fluctuation seems to change after around the time of t = 90. A shock motion raises a low frequency fluctuation. However, the shock motion in the present simulation might be unphysical because the shock wave in each passage oscillates in the same phase. As shown in Fig. 8, a quite mild and small fluctuation of mass flow rate seems to be responsible for the shock motion, but doesn't have a large effect on the flow phenomena with high frequency because of its extremely low frequency.

The time-frequency analysis has been executed based on wavelet transform. Figure 11 shows wavelet transforms of the pressure fluctuation on the blade pressure surface of R4. The Morlet wavelet transform was used as mother wavelet. There are two predominant frequencies around 10 kHz and 6 kHz. Since the blade passing frequency (BPF) of the compressor rotor is 10.3 kHz, these frequencies correspond to about 100% BPF and 60% BPF, respectively. In both of L1 and L2, the predominant frequency indicates a gradual transition from 10 kHz at the beginning to 6 kHz at the end.

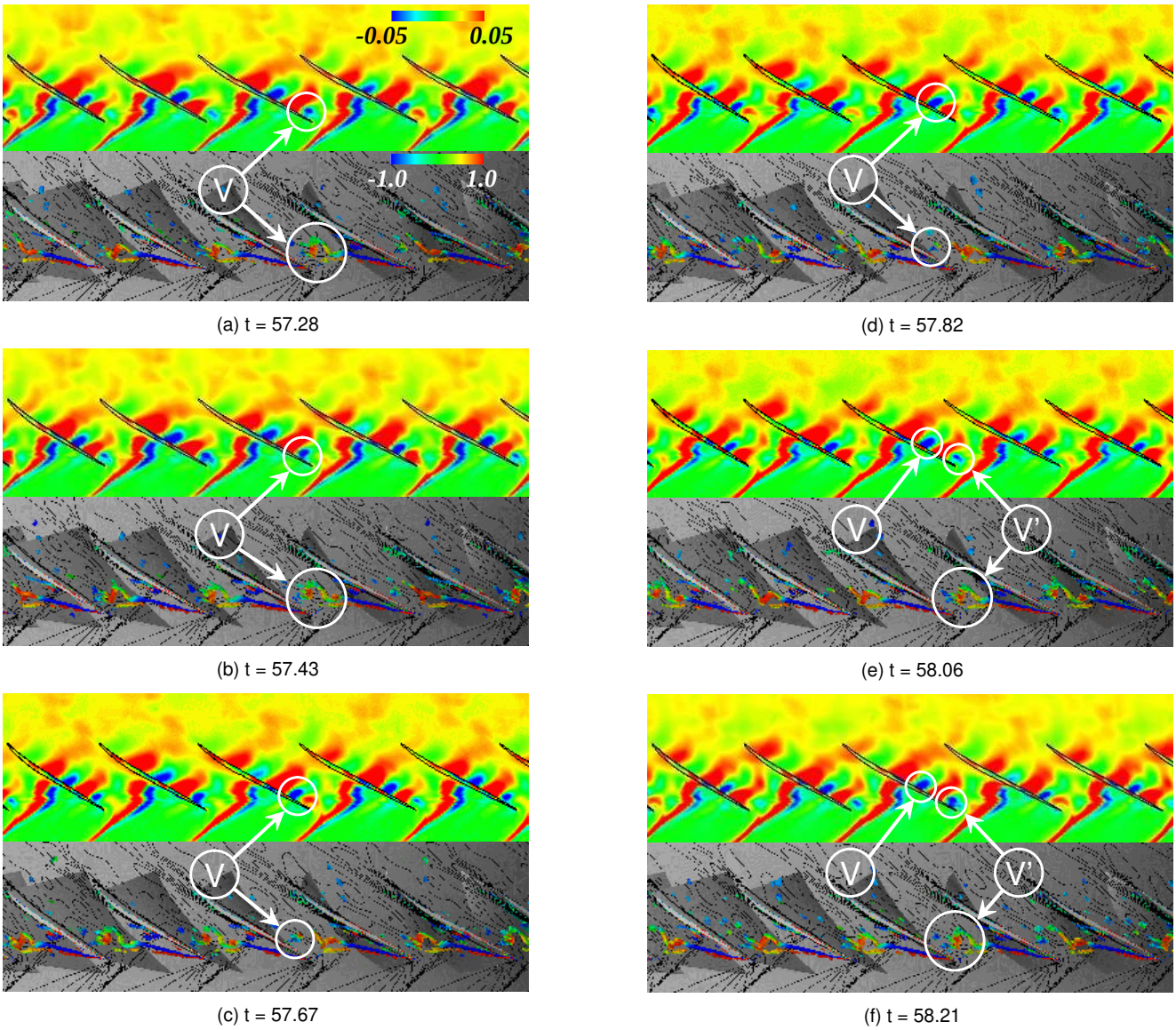

(a) t = 57.28 (d) t = 57.82

(b) t = 57.43 (e) t = 58.06

(c) t = 57.67 (f) t = 58.21

Figure 12. Time variation of fluctuation pressure distribution on the casing wall and vortical flow structure in the rotor (t = 57.28 $\sim$ 58.21)

The wave with frequency of 10 kHz is identified as the self-induced oscillation due to the vortex breakdown of the tip leakage vortex since there is no rotating disturbance at the beginning of the simulation at 88% mass flow rate. On the other hand, the wave with frequency of 6 kHz is expected to indicate occurrence of a disturbance propagating through the rotor, i.e. a rotating disturbance because it is different from the self-induced oscillation due to the vortex breakdown of the tip leakage vortex. This means that the self-induced oscillation of the tip leakage vortex due to the vortex breakdown gives rise to a rotating disturbance, and the unsteadiness in the rotor passage was switched from the self-induced oscillation mode to the rotating disturbance mode. The wave of 6 kHz shows up at L1 in advance of L2. The rotating disturbance might have emerged from around the leading edge of the rotor. First, the wave with frequency of 6 kHz is discussed.

Figure 12 shows fluctuation pressure distributions on the casing wall and instantaneous vortical flow structures in the rotor between t = 57.28 and t = 58.21. The tip leakage vortex fluctuates with time downstream of the shock wave due to the vortex breakdown. Although the tip leakage vortex breakdown is bubble-type in the steady-state simulation at 92% mass flow rate as shown in Fig. 7, it has changed to spiral-type in the unsteady simulation at 88% mass flow rate. The fluctuation of the tip leakage vortex generates an unsteadiness in the rotor passage. At the same time, the fluctuation brings about the interaction of the tip leakage vortex with the adjacent blade (see V in the figure). As shown in

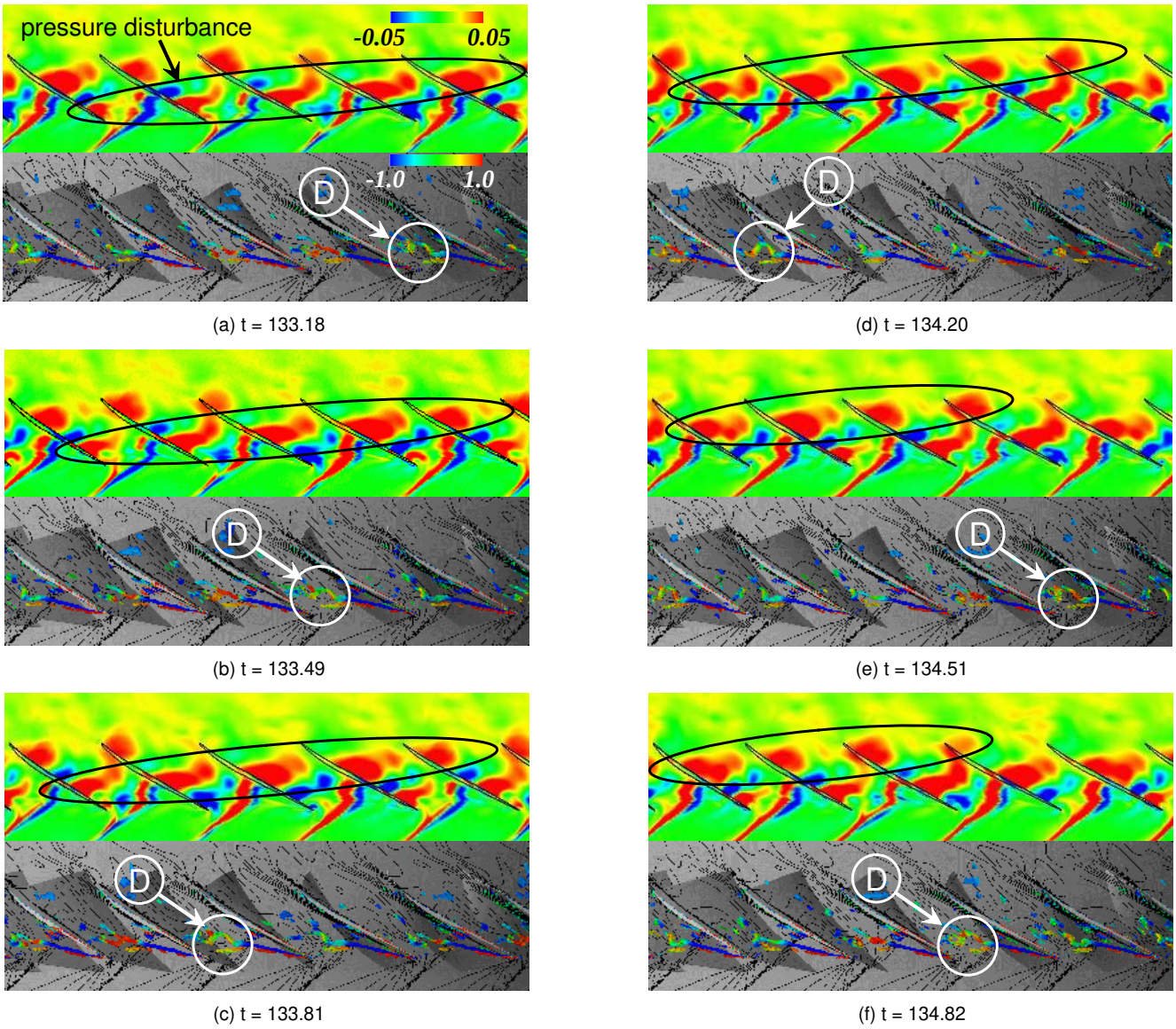

Figure 13. Time variation of fluctuation pressure distribution on the casing wall and vortical flow structure in the rotor (t = 133.18 $\sim$ 134.82)

the pressure distribution on the casing wall, a low pressure region appears around the leading edge of the pressure side due to the presence of the tip leakage vortex, and a high pressure region emerges just upstream of the low pressure region because of a blockage effect of the tip leakage vortex. Another fluctuation pressure is found near the shock wave since the shock wave moves slowly. The tip leakage vortex flows downstream along the pressure side of the adjacent rotor blade after interacting with the blade. The interaction is periodical, and its periodic time turn out to be about 0.93 since the time t = 57.28 is similar to the time t = 58.21 in vortical flow structure. The period of 0.93 corresponds with the periodic time of the high frequency fluctuation seen in Fig. 10. Therefore, the fluctuation of the tip leakage vortex can account for the high frequency fluctuation. The vortical flow structure in the rotor is slightly different in each passage, even though there seems to be no rotating disturbance and the unsteady simulation starts from the same initial condition of the steady-state solution from the single passage simulation in each passage. This is because of the initial disturbance introduced into the simulation.

The interaction of the tip leakage vortex and the adjacent blade has an impact on the tip leakage flow from the adjacent blade. Hence, the interaction affects the fluctuation of the tip leakage vortex, that is to say, the unsteadiness of flow field in the adjacent blade passage. It implies that a disturbance associated with the fluctuation of the tip leakage vortex can propagate

through the rotor, as in the case of the rotating instability. The change in the dominant frequency shown in Fig. 11 also suggests this.

Relation between Unsteady Behavior of Tip Leakage Vortex and Rotating Disturbance

For the tip clearance that is larger than 2% of blade tip chord, the rotating instability was observed [11]. As mentioned above, the vortex breakdown has a possibility to induce the disturbance like the rotating instability, and it occurred even for the relative small tip clearance because of the interaction of the tip leakage vortex with the shock wave produced in the transonic compressor rotor. Therefore, in the transonic compressor rotor, it is possible for the rotating instability to emerge even in the case of the relative small tip clearance.

Figure 13 shows a time variation of fluctuation pressure distribution on the casing wall and vortical flow structures in the rotor between t = 133.18 and t = 134.82. At this time after passing t = 90, the unsteady flow phenomena with frequency of 6 kHz is dominant and the disturbance is expected to be present. The vortical flow structures are much different in each passage as compared to Fig. 12. In addition, the same seems to be equally true of the shock motion. There are large and small fluctuations of the tip leakage vortex among all the passages. This means that the size of the vortex breakdown is different in each passage. At t = 133.18, the fluctuation pressure near the shock wave indicates negative in the passages of P1 and P4. The explanation is that the shock wave was moving downstream due to reduced-size vortex breakdown in these passages. The vortical flow structures at t = 133.49 seem as if those at t = 133.18 has traveled only one passage to the opposite rotational direction. Moreover, the vortical flow structures at two time instants of t = 133.18 and t = 134.51 extremely resemble each other (see D: D presents the tip leakage vortex greatly fluctuating in the rotor passages). It can be said that a different size of the vortex breakdown distributes in the pitchwise direction and propagates in the rotor.

The interaction of the tip leakage vortex with the adjacent blade can produce such circumferential distribution of the size of vortex breakdown. The pressure difference between the pressure and suction surface drops near the leading edge of the rotor tip, the moment the tip leakage vortex interacts with the adjacent blade, as shown in the fluctuation pressure distributions. This local drop of the blade loading weakens the swirl intensity of the tip leakage vortex, which result in a reduction in the size of vortex breakdown. As the size of vortex breakdown decreases, the fluctuation of the tip leakage vortex becomes small, and then the interaction with the adjacent blade becomes weak. Contrary to this, the weak interaction of the tip leakage vortex with the adjacent blade leads to an increased size of vortex breakdown. In this way, the circumferential distribution of the size of vortex breakdown is generated and rotates in the opposite rotational direction

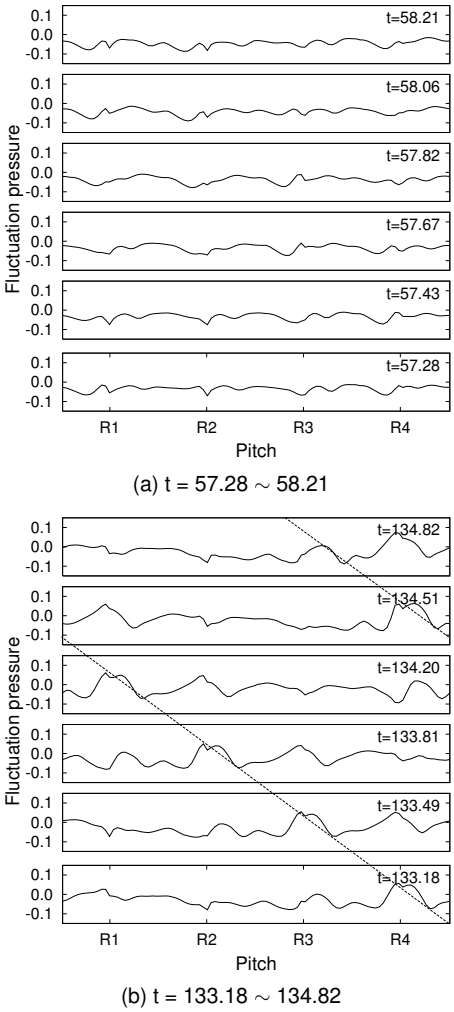

Figure 14. Time variation of fluctuation pressure distribution on the casing wall just downstream of the rotor

in the rotor. The pressure disturbance shown in the figure resulted from the propagation of such circumferentially-distributed vortex breakdown size. This explanation is similar to that for the rotating instability. Unlike the rotating instability, however, the size of vortex breakdown isn't always large or small every two passages.

Figure 14 shows a time variation of fluctuation pressure distribution on the casing wall just downstream of the rotor. This figure is shown in the relative frame of reference. In this time period between t = 133.18 and 134.82, a similar wave pattern was observed at each time and seemed to move with time toward left side in the adverse direction to the rotor rotation. This suggests an occurrence of the rotating disturbance. On the other hand, there is no such indications in the time between t = 57.28 and t = 58.21. The rotating disturbance was produced by the way mentioned above but not immediately after launching the sim-

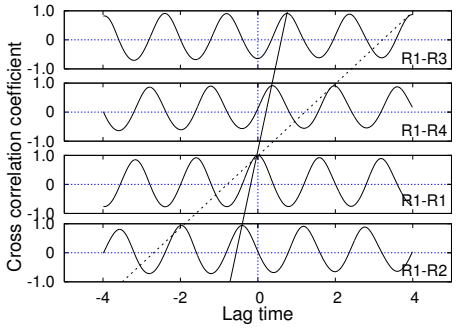

(a) L1

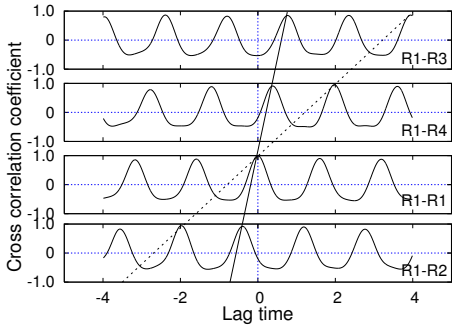

(b) L2

Figure 15. Cross correlation coefficient of pressure fluctuations on the pressure surface (t = 127.8 $\sim$ 143.4)

ulation; namely, it took about 90 non-dimensional time for the disturbance to fully develop.

Figure 15 shows cross correlation coefficients between the rotor blade R1 and the other blades. The cross correlation coefficient was calculated from the pressure fluctuations between t = 127.8 and 143.4. The lag time in the abscissa axis was normalized by the blade passing period. It should be noted that the pressure fluctuations were obtained in the relative frame. The cross correlation coefficient becomes high in the order of R1-R4, R1-R3, R1-R2. This means the propagation of the pressure disturbance in the adverse direction to the rotor rotation. In R1-R4, the first highest correlation appeared at the time lag of 0.4. This means that the disturbance propagated one rotor pitch from R1 to R4 during this time (solid line). Consequently, the propagation speed of the disturbance was calculated to be about 2.5 times the rotor speed in the relative frame. The cross correlation had the highest value only once while the disturbance with this speed propagated across the four rotor passages. Therefore, the wavelength was found to be four pitch of the rotor. Considering that the rotating disturbance was caused by the flow fluctuation due to the vortex breakdown as mentioned above, this propagation speed was too fast. It was also so fast in comparison with that of the rotating instability. A plausible explanation was that the lag time for the R1-R4 cross correlation was not 0.4 but 2 at the

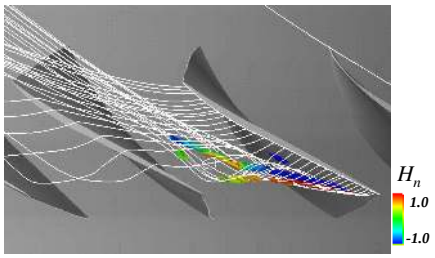

Figure 16. Tip leakage streamlines and vortical flow structures in the time-averaged flow field between t = 93.5 and t = 120.0

subsequent second peak (dashed line). Assuming like this, the disturbance propagated one rotor pitch during two pitch rotation of the rotor; namely the propagation speed was half of the rotor speed in the relative frame. The disturbance rotated 50% of the rotor speed in the absolute frame, which correspond to that of the rotating instability. In this case, the wavelength of the disturbance was one rotor pitch.

It should be noted that the wavelength might have been influenced by the computational domain in the present unsteady simulation. In numerical simulations, it is considered that the size of computational domain, i.e. the number of passages to be computed, have a potential to attract the mode of the disturbances depending on the size. As for the propagation speed and wavelength of the disturbance, these might be different from those of real phenomena in the compressor rotor. However, it is true that the rotating disturbance has been induced by the tip leakage vortex breakdown although it is a finding from the four-passage simulation. The present simulation implies a possible occurrence of rotating disturbances, which is induced by the vortex breakdown, in compressors.

The rotating disturbance observed in the present work is interpreted as follows. The tip leakage vortex fluctuates due to the vortex breakdown and interacts with the adjacent blade tip near the leading edge. Therefore, the pressure difference between the pressure and suction surfaces fluctuates; namely, the tip leakage flow fluctuates. Since this fluctuation was transmitted to the adjacent blade passage via the tip leakage vortex fluctuation, it has a time lag between the adjacent blade passages. As a result, a kind of feedback loop system was constructed and the rotating disturbance was produced in the rotor.

Time-averaged Flow Field

The time-averaged flow field between t = 93.5 and t = 120.0 is shown in Fig. 16. The figure shows tip leakage streamlines as well as vortical flow structures in the rotor. As mentioned above, 'spillage' and 'backflow' have been proposed as the criteria for the spike stall [7]. These flow phenomena are absent in the present simulation. Therefore, the disturbance observed in the present simulation is different from a spiky short length-

scale disturbance and occurs in the stable operating range before the stall. In addition, as described above, the fluctuation of the tip leakage vortex due to the vortex breakdown induced the disturbance, and also produced a large pressure fluctuation in the rotor passage around the pressure side of the leading edge. These features are similar to those of the rotating instability.

CONCLUSIONS

Unsteady behaviors of tip clearance flow at a near-stall condition and the relation between such unsteadiness and a rotating disturbance have been investigated by multi-passage URANS simulations for a transonic axial compressor rotor. The results are summarized as follows:

1. In the compressor rotor, the vortex breakdown happens in the tip leakage vortex at near-stall condition. The tip leakage vortex fluctuates downstream of the shock wave, interacting with the adjacent blade near the leading edge. The vortex breakdown gives rise to an unsteadiness in the rotor passage.
2. At a condition of less mass flow rate, the interaction of the tip leakage vortex with the adjacent blade is enhanced by an amplified fluctuation of the tip leakage vortex. A size of the vortex breakdown begin to differ among each passage due to a variation of local blade loading near the rotor tip. This rotates in the rotor, which results in a rotating disturbance.
3. This disturbance emerges before stall. The propagation mechanism and features of the disturbance are similar to those of the rotating instability.

ACKNOWLEDGMENT

The present research was partially supported by Japan Society for the Promotion of Science (JSPS), Grant-in-Aid for Young Scientists (B), KAKENHI 19760107, 2007.

REFERENCES

[1] Day, I. J., 1993. "Stall inception in axial flow compressors". *ASME J. Turbomachinery,* **115**, pp. 1–9.

[2] Garnier, V. H., Epstein, A. H., and Greitzer, E. M., 1991. "Rotating waves as a stall inception indication in axial compressors". *ASME J. Turbomachinery,* **113**, pp. 290–301.

[3] McDougall, N. M., Cumpsty, N. A., and Hynes, T. P., 1990. "Stall inception in axial compressors". *ASME J. Turbomachinery,* **112**, pp. 116–125.

[4] Camp, T. R., and Day, I. J., 1998. "A study of spike and modal stall phenomena in a low-speed axial compressors". *ASME J. Turbomachinery,* **120**, pp. 393–401.

[5] Hoying, D. A., Tan, C. S., Vo, H. D., and Greitzer, E. M., 1999. "Role of blade passage flow structures in axial compressor rotating stall inception". *ASME J. Turbomachinery,* **121**, pp. 735–742.

[6] Hah, C., Schulze, R., Wagner, S., and Hennecke, D. K., 1999. "Numerical and experimental study for short wavelength stall inception in a low-speed axial compressor". ISABE. Paper No. 99-7033.

[7] Vo, H. D., Tan, C. S., and Greitzer, E. M., 2005. "Criteria for spike initiated rotating stall". ASME. GT2005-68374.

[8] Day, I. J., Breuer, T., Escuret, J., Cherrett, M., and Wilson, A., 1999. "Stall inception and the prospects for active control in four high speed compressors". *ASME J. Turbomachinery,* **121**, pp. 18–27.

[9] Inoue, M., Kuroumaru, M., Tanino, T., Yoshida, S., and Furukawa, M., 2001. "Comparative studies on short and long length-scale stall cell propagating in an axial compressor rotor". *ASME J. Turbomachinery,* **123**(1), pp. 24–32.

[10] Inoue, M., Kuroumaru, M., Yoshida, S., and Furukawa, M., 2002. "Short and long length-scale disturbances leading to rotating stall in an axial compressor stage with different stator-rotor gaps". *ASME J. Turbomachinery,* **124**(3), pp. 376–384.

[11] Mailach, R., Lehmann, I., and Vogeler, K., 2001. "Rotating instabilities in an axial compressor originating from the fluctuating blade tip vortex". *ASME J. Turbomachinery,* **123**, pp. 453–463.

[12] Furukawa, M., Inoue, M., Saiki, K., and Yamada, K., 1999. "The role of tip leakage vortex breakdown in compressor rotor aerodynamics". *ASME J. Turbomachinery,* **121**(3), pp. 469–480.

[13] Furukawa, M., Saiki, K., Yamada, K., and Inoue, M., 2000. "Unsteady flow behavior due to breakdown of tip leakage vortex in an axial compressor rotor at near-stall condition". ASME. Paper No. 2000-GT-666.

[14] Inoue, M., Kuroumaru, M., Iwamoto, T., and Ando, Y., 1991. "Detection of a rotating stall precursor in isolated axial flow compressor rotors". *ASME J. Turbomachinery,* **113**(2), pp. 281–289.

[15] Yamada, K., Furukawa, M., Nakano, T., Inoue, M., and Funazaki, K., 2004. "Unsteady three-dimensional flow phenomena due to breakdown of tip leakage vortex in a transonic axial compressor rotor". In ASME. GT2004-53745.

[16] Yamada, K., Funazaki, K., and Furukawa, M., 2007. "The behavior of tip clearance flow at near-stall condition in a transonic axial compressor rotor". In ASME. GT2007-27725.

[17] Reid, L., and Moore, R. D., 1978. "Design and overall performance of four highly-loaded, high-speed inlet stages for an advanced, high-pressure-ratio core compressor". NASA. TP-1337.

[18] Suder, K. L., and Celestina, M. L., 1996. "Experiment and computational investigation of the tip clearance flow in a transonic axial compressor rotor". *ASME J. Turbomachinery,* **118**, pp. 218–229.

[19] Strazisar, A. J., and Denton, J. D., 1995. "Cfd code as-

sessment in turbomachinery - a progress report". In IGTI Global Gas Turbine News, pp. 12–14.
[20] Chima, R. V., 1998. "Calculation of tip clearance effect in a transonic compressor rotor". *ASME J. Turbomachinery,* **120**, pp. 131–140.
[21] Hah, C., and Loellbach, J., 1999. "Development of hub corner stall and its influence on the performance of axial compressor blade rows". *ASME J. Turbomachinery,* **121**, pp. 67–77.
[22] Suder, K. L., 1998. "Blockage development in a transonic, axial compressor rotor". *ASME J. Turbomachinery,* **120**(3), pp. 465–476.
[23] Furukawa, M., Nakano, T., and Inoue, M., 1992. "Unsteady navier-stokes simulation of transonic cascade flow using an unfactored implicit upwind relaxation scheme with inner iterations". *ASME J. Turbomachinery,* **114**(3), pp. 599–606.
[24] Inoue, M., and Furukawa, M., 1994. "Artificial dissipative and upwind schemes for turbomachinery blade flow calculation". VKI Lecture Series. No. 1994-06.
[25] Shima, E., and Jounouchi, T., 1997. "Role of cfd in aeronautical engineering (no.14)-ausm type upwind schemes". In the 14th NAL Symposium on Aircraft Computational Aerodynamics, National Aerospace Lab., pp. 7–12. NAL SP-34.
[26] Anderson, W. K., Thomas, J. L., and van Leer, B., 1986. "Comparison of finite volume flux vector splittings for the euler equations". *AIAA Journal,* **24**(9), pp. 1453–1460.
[27] Wilcox, D. C., 1994. "Simulation of transition with a two-equation turbulence model". *AIAA Journal,* **32**(2), pp. 247–255.
[28] Chakravarthy, S. R., 1984. "Relaxation method for unfactored implicit upwind schemes". AIAA. Paper No. 84-0165.
[29] Chen, J. P., Hathaway, M. D., and Herrick, G. P., 2007. "Pre-stall behavior of a transonic axial compressor stage via time-accurate numerical simulation". ASME. GT2007-27926.
[30] Hah, C., Bergner, J., and Schiffer, H., 2006. "Short length-scale rotating stall inception in a transonic axial compressor - criteria and mechanisms". ASME. GT2006-90045.
[31] Sawada, K., 1995. "A convenient visualization method for identifying vortex centers". *Japan Soc. of Aero. Space Sci.,* **38**(120), pp. 102–116.
[32] Shabbir, A., Celestina, M., Adamczyk, J., and Strazisar, A., 1997. "The effect of hub leakage flow on two high speed axial flow compressor rotors". ASME. Paper No. 97-GT-346.